# Modeling of As$_2$S$_3$ Raman Fiber Lasers Operating in the Mid-Infrared
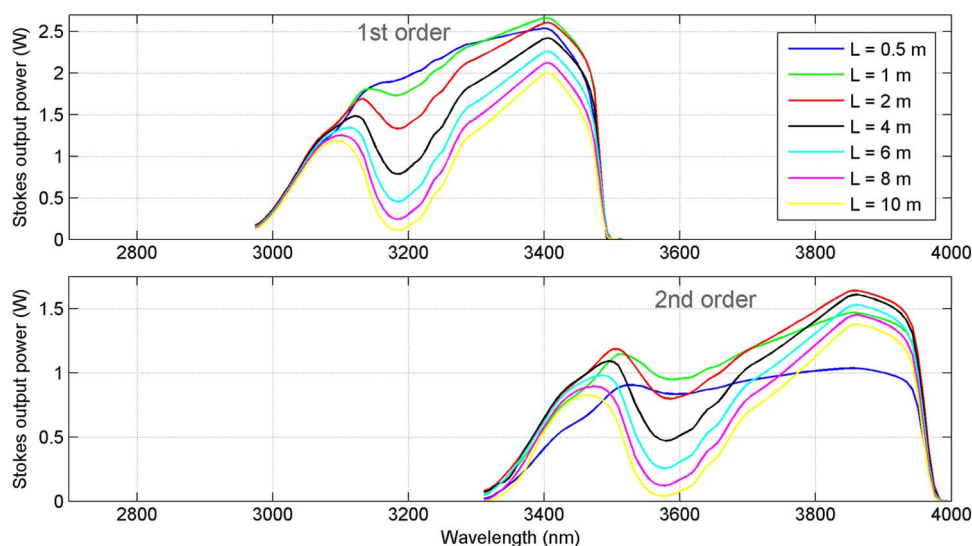
Vincent Fortin
Martin Bernier
Mohammed El-Amraoui
Younès Messaddeq
Réal Vallée

# Modeling of As$_2$S$_3$ Raman Fiber Lasers Operating in the Mid-Infrared

**Vincent Fortin, Martin Bernier, Mohammed El-Amraoui, Younès Messaddeq, and Réal Vallée**

Center for Optics, Photonics, and Lasers (COPL), Université Laval, Québec, QC G1V 0A6, Canada

**Abstract:** A numerical study of As$_2$S$_3$ Raman fiber lasers is carried out to show their potential for the entire coverage of the 3–4-$\mu$m spectral band. Experimental results are first obtained from such a laser operated under controlled conditions in order to set the fiber parameters (i.e., gain and attenuation coefficients) to be used in the numerical model. An exhaustive numerical analysis is then performed to establish the conditions for optimum lasing performances over the entire 3–4-$\mu$m spectral band.

**Index Terms:** Fiber lasers, Raman fiber lasers, mid-infrared lasers, chalcogenide fiber, modeling.

## 1. Introduction

Generation of coherent radiation in the 2–20 $\mu$m wavelength range holds great promises for various application fields including spectroscopy/environment, surgery/medicine as well as countermeasures. Fiber lasers are potential candidates for such applications where high power, superior beam quality and ruggedness are generally required. However, the long-wavelength limited transparency of standard silica glass fibers restricts their wavelength coverage to less than 2.1 $\mu$m. The use of low phonon glass hosts (i.e., fluoride and chalcogenide glasses) possessing an extended transmission window is an interesting alternative to that problem. However, low-phonon energy glass fiber lasers doped with rare-earth ions are currently limited to fluoride glass fibers and actually offer only a few emission bands, which become increasingly scarce at wavelengths longer than 3 $\mu$m. Raman Fiber Lasers (RFLs), which can be implemented from either fluoride or chalcogenide fibers, provide an efficient solution to fill the wavelength gaps where no other fiber laser can operate. Moreover, the Raman fiber laser overall assembly, including the pump laser cavity and the Raman cavity itself, can be made entirely monolithic once fiber Bragg gratings (FBGs) inscription and fusion splices are mastered.

In recent years, it was demonstrated that radiation in the vicinity of 2.1–2.3 $\mu$m could be generated using a fluoride glass based Raman fiber laser consisting of a pair of FBGs directly written inside a low-loss fluoride fiber and pumped by a Tm:silica fiber laser [1], [2]. More recently, a first-order As$_2$S$_3$ Raman fiber laser was demonstrated for the first time, delivering a 600 mW peak power at 3340 nm [3]. This demonstration relied on recent progresses in the development of powerful and reliable erbium doped fluoride glass fiber lasers operating near 3 $\mu$m [4].

The aim of this paper is to demonstrate that the entire spectrum from 3 to 4 $\mu$m could be covered using the combination of first- and second-order chalcogenide (As$_2$S$_3$) based RFLs. First, the details

of the RFL numerical model are presented. Then, we estimate the Raman gain and Stokes attenuation coefficient using experimental results obtained from a specially designed Raman fiber laser cavity. Finally, we show that high efficiencies can be expected when the fiber length and output coupler reflectivity are properly optimized.

## 2. Raman Fiber Laser Model

Our numerical study of the chalcogenide RFL is based on the standard power coupled equations for Raman lasers, as described in [5]. In this equation set, we treat the pump and Stokes (1st and 2nd) as monochromatic signals an suppose the power transfer occurs only between two successive orders. We also neglect polarization effects and the spontaneous Raman scattering contribution. Two equations are used for each wavelength to describe forward $(+)$ and backward $(-)$ propagation, respectively. For a second-order Raman fiber laser, the equation set can be written as:

$$\frac{dP_0(z)^{\pm}}{dz} = \mp \alpha_0 P_0(z)^{\pm} \mp \frac{\lambda_1}{\lambda_0} \frac{g_{R0}}{A_{\text{eff0}}} x_{0-1} \left( P_1(z)^+ + P_1(z)^- \right) P_0(z)^{\pm}$$

$$\frac{dP_1(z)^{\pm}}{dz} = \mp \alpha_1 P_1(z)^{\pm} \pm \frac{g_{R0}}{A_{\text{eff0}}} x_{0-1} \left( P_0(z)^+ + P_0(z)^- \right) P_1(z)^{\pm}$$

$$\mp \frac{g_{R1}}{A_{\text{eff1}}} x_{1-2} \frac{\lambda_2}{\lambda_1} \left( P_2(z)^+ + P_2(z)^- \right) P_1(z)^{\pm}$$

$$\frac{dP_2(z)^{\pm}}{dz} = \mp \alpha_2 P_2(z)^{\pm} \pm \frac{g_{R1}}{A_{\text{eff1}}} x_{1-2} \left( P_1(z)^+ + P_1(z)^- \right) P_2(z)^{\pm} \qquad (1)$$

with boundary conditions given by

$$P_0(0)^+ = P_{\text{launched}}$$
$$P_0(L)^- = R_{\text{out0}} P_0(L)^+$$
$$P_1(0)^+ = R_{\text{in1}} P_1(0)^-$$
$$P_1(L)^- = R_{\text{out1}} P_1(L)^+$$
$$P_2(0)^+ = R_{\text{in2}} P_2(0)^-$$
$$P_2(L)^- = R_{\text{out2}} P_2(L)^+ \qquad (2)$$

where the indices 0, 1, and 2 refer to the pump, first-order Stokes, and second-order Stokes respectively, $g_{R,i}$ is the Raman gain coefficient, $A_{\text{eff},i}$ is the effective area of the LP$_{01}$ mode of the fiber, $x_{i-j}$ is the correction from the modal overlap (between LP$_{01}$ modes at $\lambda_i$ and $\lambda_j$ wavelengths) and $\alpha_i$ is the attenuation coefficient. In addition, $R_{\text{in},i}$ and $R_{\text{out},i}$ correspond to the reflectivity of the input and output fiber Bragg gratings (FBGs). Note that first-order equations can be found by setting $P_2(z)^{\pm} = 0$. The coupled equations are solved in Matlab using a finite difference code that implements a three-stage Lobatto IIIa formula which provide a fourth-order accuracy.

It is well known that spectral broadening inside a RFL cavity has a significant impact on laser performances [6]–[10]. In fact, it reduces the FBG effective reflectivity by causing a portion of the intracavity power to leak outside the cavity. These effects are not readily accounted for in Eqs. (1) and (2). However, in some cases where experimental data on the FBG and laser spectra are available (as a function of the output power), the impact on the reflectivity can be implemented by calculating the effective reflectivity $R_{\text{eff}}$ with the following integrals:

$$R_{\text{eff}} = \frac{P_{\text{reflected}}}{P_{\text{incident}}} = \frac{\int \frac{P_{\text{out}}(\lambda)}{1-R_{\text{out}}(\lambda)} R_{\text{out}}(\lambda) d\lambda}{\int \frac{P_{\text{out}}(\lambda)}{1-R_{\text{out}}(\lambda)} d\lambda}. \qquad (3)$$

Note that it is not always possible to perform this calculation for every FBGs involved. For instance, we do not have access to the spectrum leaking from the input grating as it would require a
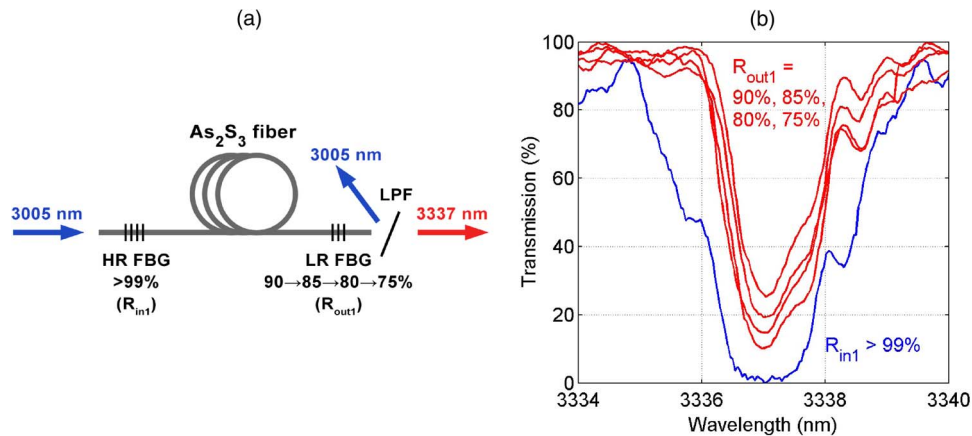
Fig. 1. (a) Experimental setup of the As$_2$S$_3$ first-order RFL. (b) Spectrum of the FBGs.

setup that is specifically designed for this purpose. Moreover, even when the effective reflectivity calculation is performed on a specific Raman cavity; the results cannot be readily transposed to different cavity parameters (e.g., fiber length, output coupler reflectivity, FBG bandwidth, etc.). Therefore, we chose not to include the effective reflectivity effects in the last section of this paper, where predictions are made for a wide range of first- and second-order RFLs parameters. Such approximation is justified for situations where the power leakage is minimized with the use of broadband (i.e., chirped) FBGs [9].

## 3. Validation of the Model Using Experimental Results

Reliable numerical predictions of chalcogenide RFLs critically rely on accurate values of both the fiber Raman gain and attenuation coefficients. While the attenuation of our single-mode fiber was previously measured in a cutback procedure [11], a significant amount of diffusion points (i.e., point defects) were later revealed when the residual fiber segment was screened using an InSb IR camera (Telops TEL-3306). The losses associated to these point defects were found to be responsible for a significant part of the overall (average) attenuation coefficient. For the present experiment, we have carefully selected a fiber segment without defects and thus, a significantly lower attenuation than previously reported (100 dB/km) is expected.

The experimental setup used for the model validation experiments consists of a 1.8 meter defect-free As$_2$S$_3$ fiber in which two first-order Stokes FBGs are written (shown in Fig. 1). The output FBG has an initial value (right after inscription) of about 90%. To obtain a better estimation of the Raman gain and Stokes attenuation, the output FBG was subsequently heated to lower its reflectivity from 90% to 85%, to 80% and finally to 75%, corresponding to four distinct Raman cavities. The FBGs spectral responses are shown in Fig. 1(b). The chalcogenide fiber has a 4/150 $\mu$m (core/clad) diameter and a numerical aperture of 0.36, leading to a cutoff wavelength of about 1900 nm. A 3005 nm Er:ZBLAN fiber laser operated in quasi-CW regime is used to pump the Raman cavity (see Ref. [12] for details). Note that this wavelength is the longest ever reported from an erbium-doped fiber laser. This laser delivers 5 ms pulses at a repetition rate of 20 Hz which are sufficiently long for the RFL to reach its steady state. The difference between the pump and Stokes wavelengths (i.e., 3005 and 3337 nm) corresponds to a frequency shift of 331 cm$^{-1}$.

The average power is measured with a thermopile detector (Gentec XLP12-3S-H2) and the corresponding peak power is inferred from the pulse precise temporal shape [3]. To separate the Stokes signal from the pump, an in-house fabricated long pass filter is placed before the detector. The Stokes spectrum as well as the FBG transmission spectra are measured using a grating-based scanning spectrometer (Digikrom DK480) coupled to a nitrogen-cooled InSb detector (Judson, J10D-M204-R01M-60).
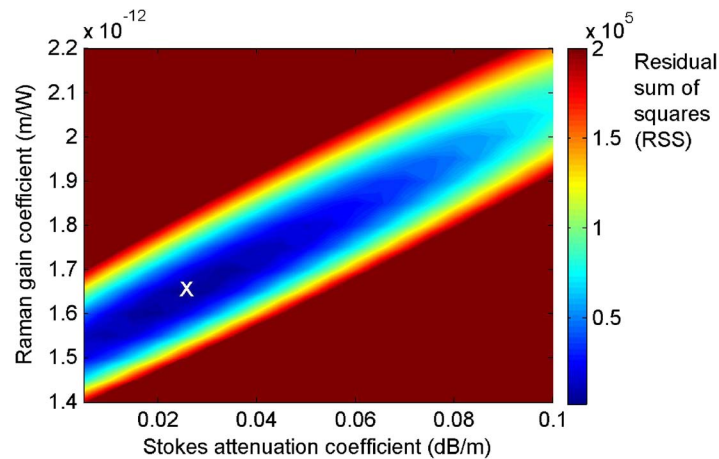
Fig. 2. Residual sum of squares between numerical and experimental laser thresholds as a function of the Stokes attenuation and the Raman gain coefficient. Least error is denoted by a white cross.
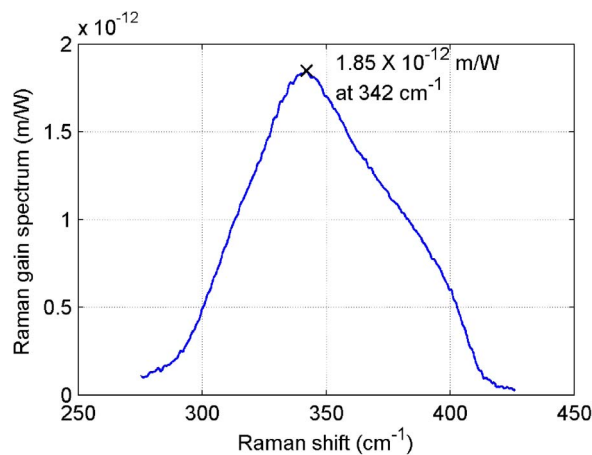


Fig. 3. Raman gain spectrum of the single-mode As$_2$S$_3$ fiber measured by pump-probe experiment, as in [1].

Numerical calculations based on Eqs. (1) and (2) are performed to fit the fiber attenuation and Raman gain coefficients. For each simulation, we first calculate the sum of squared errors between experimental and numerical laser thresholds (for the four laser cavities). To replicate the experimental conditions, the simulations data is corrected to account for the attenuation of the fiber prior and after the laser cavity, for the Fresnel reflection of the fiber tip and for the losses associated with the long pass filter. We notice the existence of a family of parameter sets that give a reasonable fit of the laser thresholds (Fig. 2). Accordingly, the least error is obtained for $\alpha_1 = 0.025$ dB/m and $g_R = 1.65 * 10^{-12}$ m/W (unpolarized). Since the operating wavelength is slightly shifted from the measured Raman gain peak of our fiber, at 342 cm$^{-1}$ (see Fig. 3), the peak value is estimated at $1.85 * 10^{-12}$ m/W. This value is somewhat higher than previous reports spreading from 1.07 and $1.42 * 10^{-12}$ m/W at the same wavelength (assuming a simple inverse relation with pump wavelength) [13]–[15]. Note that a variation of the gain coefficient is possible when slightly different core compositions are used.

Based on the derived values of $\alpha_1$ and $g_R$, we then computed the lasing curves. First note that in order to simultaneously fit the laser thresholds and the slope efficiencies, a power leak of up to 7% (due to spectral broadening) was introduced in the numerical simulation. This was accounted for by
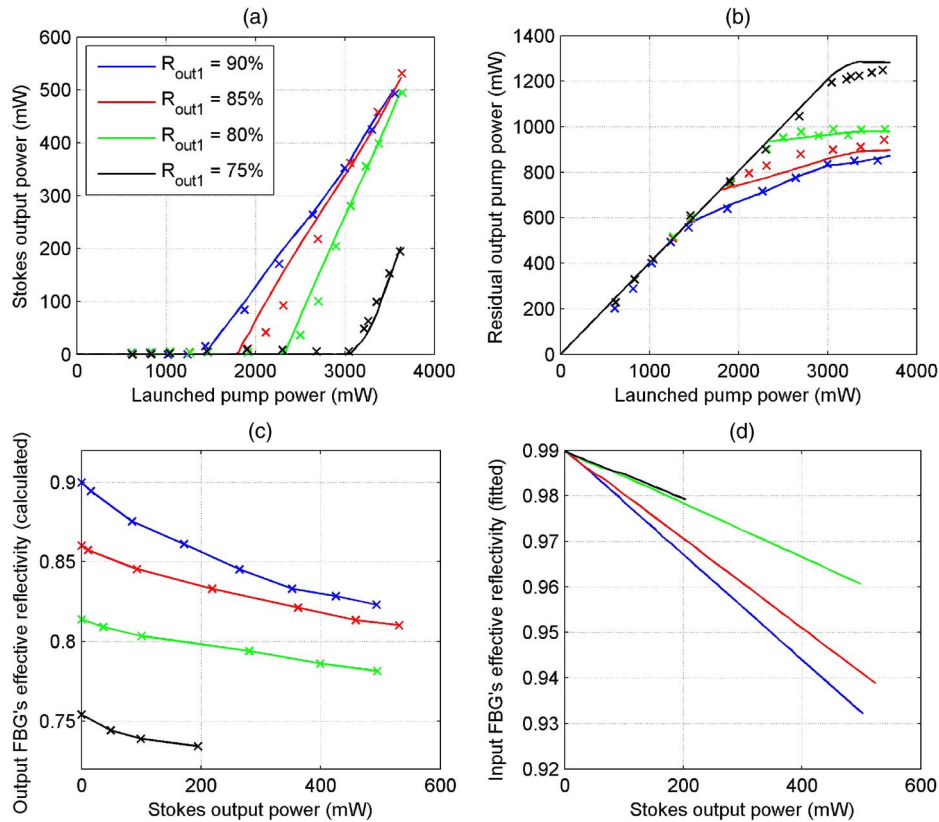
Fig. 4. (a) Stokes output peak power and (b) residual pump peak power with respect to the launched pump peak power (the x's represent experimental data points). (c) Calculated effective reflectivity associated to the output FBG [obtained using Eq. (3)]. (d) Fitted input FBG's effective reflectivity.

fitting the input FBG's effective reflectivity as a function of Stokes output power. Accordingly, Fig. 4 shows that one can reproduce quite accurately both the pump and Stokes experimental results when including the effect of spectral broadening on the FBGs effective reflectivities. As expected, Fig. 4(d) curves indicate that a higher output coupler reflectivity leads to increased power leakage through the input FBG.

## 4. Optimized First- and Second-Order RFLs Emitting Between 3 and 4 $\mu$m

Numerical simulations of optimized first- and second-order RFLs are presented in this section. Based on the actual gain/loss parameters derived in the previous section, we show the 3–4 $\mu$m spectral range could be covered provided the pump wavelength can be varied from 2700 to 3050 nm (i.e., the expected limits of an Er:ZBLAN fiber laser). For each pump wavelength, first and second Stokes order wavelengths are chosen to match the peak Raman gain coefficient at 342 cm$^{-1}$. Then, the attenuation coefficients are adjusted as well as the effective area and the Raman gain itself, which is scaled using an inverse relationship between the gain and pump wavelength. For Stokes wavelengths extending beyond the expected long wavelength limit of an Er:ZBLAN fiber laser pump (at 3050 nm), we set the pump wavelength at 3050 nm and lower the Raman gain according to the As$_2$S$_3$ Raman gain spectrum (Fig. 3).

The modeled laser cavity (see Fig. 5) consists of two pairs of FBGs, one located at the first-order Stokes wavelength and the other at the second Stokes order (where applicable). A highly reflective FBG (99%) is included to recycle the residual pump and thus improve the Raman conversion efficiency.
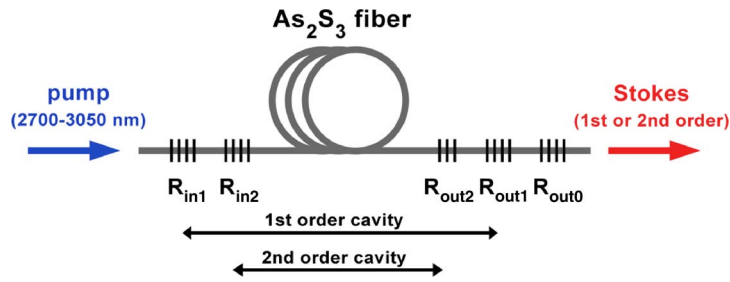
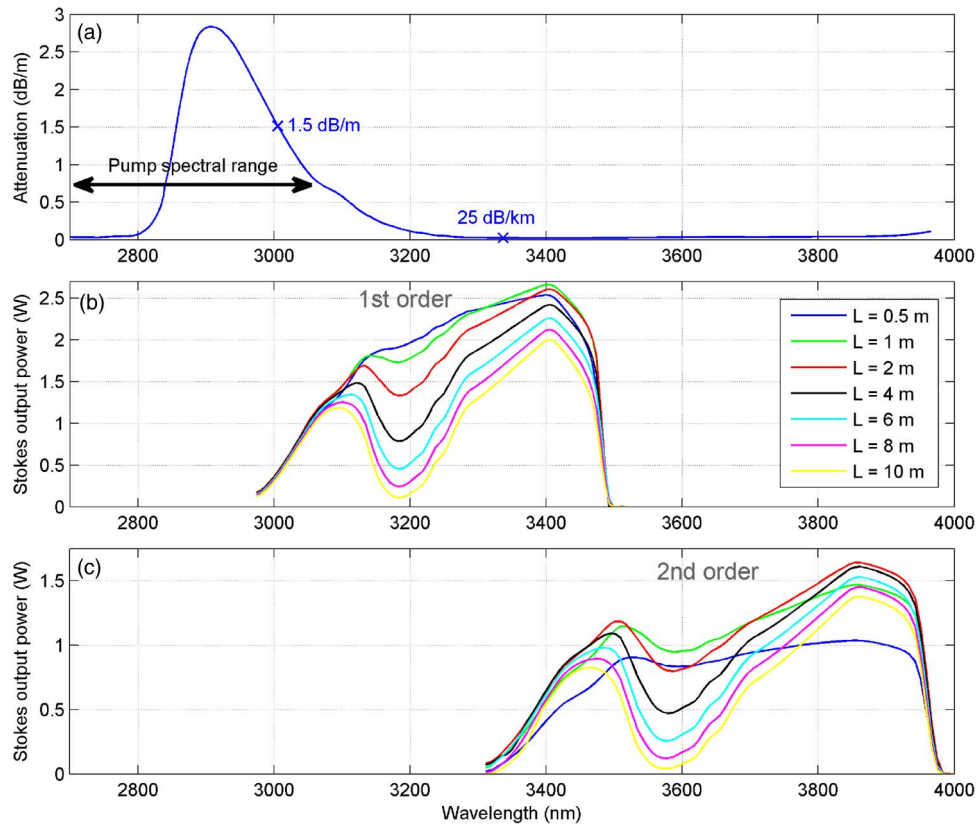Fig. 5. Schematic diagram of the modeled As$_2$S$_3$ Raman cavity.



Fig. 6. (a) Spectral attenuation of the single-mode As$_2$S$_3$ fiber showing the fitted background losses and OH absorption peak. (b) First-order and (c) second-order Stokes output power as a function of wavelength and fiber length ($P_{\text{launched}} = 5$ W).

For all the simulations, the spectral broadening effects are neglected based on the assumption that broadband FBGs could be written in As$_2$S$_3$ fibers. The value of the peak Raman gain coefficient is set to $1.85 * 10^{-12}$ m/W at 3005 nm (reference wavelength) and the background attenuation of the fiber is scaled to fit our value at 3337 nm (i.e., $\alpha_1 = 0.025$ dB/m) from the previous section. The OH absorption peak around 2.9 $\mu$m is uncoupled (numerically) from the rest of the attenuation curve and is scaled separately to have 1.5 dB/m at 3005 nm, a value obtained from a cutback experiment. The resulting attenuation curve is shown in Fig. 6(a) for the wavelength range of interest (i.e., from 2.7 to 4 $\mu$m).

Fig. 6(b) and (c) presents simulations performed for different fiber lengths at a launched pump power of 5 W. For each point, the output FBG reflectivity was simultaneously optimized to obtain the
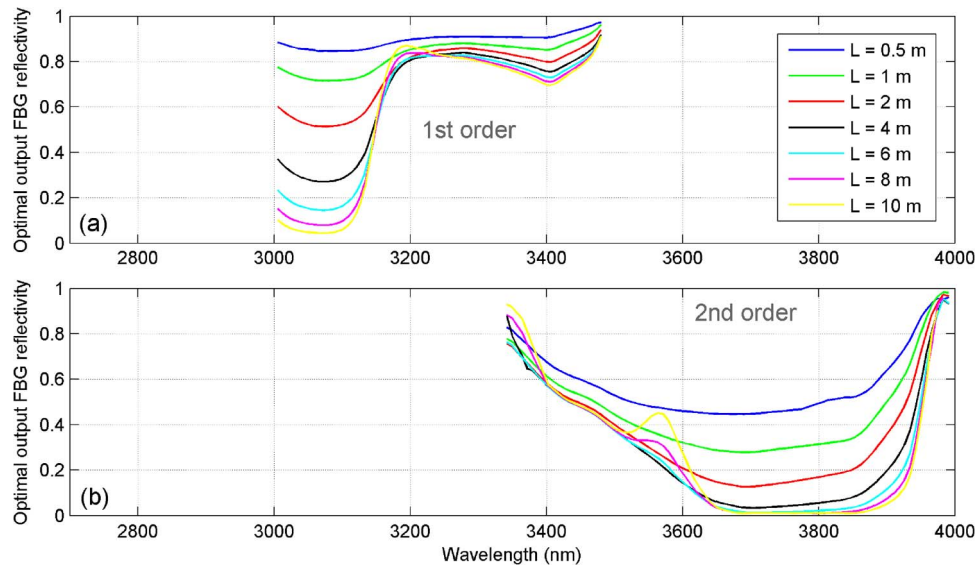
Fig. 7. Optimized output coupler's reflectivity for (a) a first-order and (b) a second-order RFL as a function of wavelength and fiber length ($P_{launched} = 5$ W).

maximum output power, as shown in Fig. 7. One should note that for long fiber segments, the power drop observed (e.g., near 3200 and 3600 nm) could be reduced using a pump wavelength shorter than the Raman peak shift, where the attenuation is lower. At this power level, the optimal length varies between 0.5 and 4 meters, depending primarily on the fiber attenuation. These lengths are significantly shorter than typical Raman cavity lengths, which are usually of the order of a few hundred meters to a kilometer [16]. This can be explained by the fact that both the Raman gain and attenuation of our chalcogenide fiber are significantly higher than for standard silicate based fibers. We also note an important variation of the optimal output coupler's reflectivity as the pump wavelength is moved between 2700 and 3050 nm. For first-order RFLs, a higher output reflectivity is needed to reach the laser threshold when the pump is near the OH absorption peak. On the other hand, second-order RFLs require higher finesse cavities for shorter pump wavelengths because the first Stokes order falls within the OH absorption peak. An increase of the optimal reflectivity is also observed outside the Er:ZBLAN pump wavelength range where the Raman gain coefficient decrease according to the gain spectrum.

Fig. 8 presents Stokes power curves with respect to the launched pump power using cavity parameters that provide the highest output power (i.e., optimized length and output coupler reflectivity). Four pump wavelengths were chosen: 2750, 2850, 2950, and 3050 nm. The slope efficiency of the laser is maximal for pump wavelengths beyond the OH peak and can reach a value of 66% for first-order and 46% for second-order cavities. On the other hand, the worst performances are obtained when pumping on the short wavelength side of the OH peak (i.e., for a 2750 nm pump). This can be explained by the fact that the corresponding first-order Stokes wave is subjected to a significantly higher attenuation. In general, the efficiencies can be improved even more by lowering the output FBG reflectivity. However, as the threshold will increase as well, a stronger pump will be required to extract a higher Stokes output power. As for the effect of the FBG used as pump reflector, it was found to play a more critical role for pump wavelengths lying between 2700 nm and 2850 nm than for those lying within the OH peak (i.e., between 2850 nm and 3000 nm) where the pump is more strongly absorbed.

A few general guidelines can be drawn from our simulations. Evidently, with a fiber having a lower attenuation, we can expect a longer optimal length and an enhanced efficiency as both pump and Stokes waves can propagate a longer distance before suffering from significant attenuation. To achieve higher output powers, one might consider the use of a chalcogenide fiber having a larger
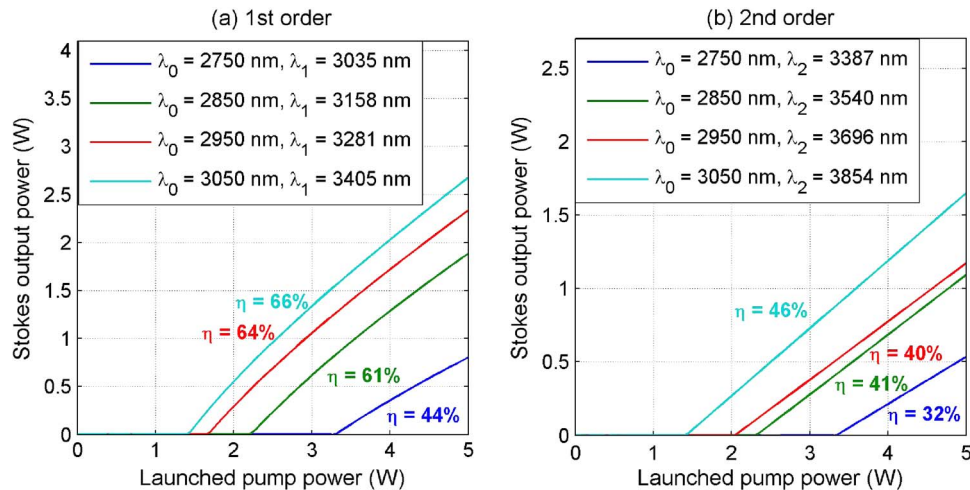
Fig. 8. Stokes output power of (a) a first-order and (b) a second-order RFL as a function of the launched pump power, using optimized length and output FBG reflectivity.

effective mode area. While this would reduce the effective Raman gain, it would also facilitate the coupling of the pump into the As$_2$S$_3$ fiber (i.e., increase the pump launch efficiency) and increase the power damage threshold substantially. For such a fiber, a higher Raman laser threshold is expected; nevertheless, the efficiency should be comparable to those of Fig. 8 if sufficient pump power is provided.

These results reveal the great potential of RFLs as compact laser sources operating in the mid-infrared. Nevertheless, to reach experimental performances comparable to the numerical ones, a few improvements are required. First, we note that the discrepancies observed between experimental and numerical efficiencies are primarily caused by significant power leaks through the FBGs. By improving our techniques to write broadband chirped FBGs, we believe the power leakage could be minimized and even become negligible [9]. A reduction of OH impurity content in these fibers would also be highly beneficial as it could raise the conversion efficiency dramatically, particularly in the low spectral range of the pump (2700–2950 nm). Calculations reveal that the thresholds could be lowered by as much as a factor of 2 if the OH absorption peak was removed.

We also note that even if our study was limited to output wavelengths between 3 and 4 $\mu$m, longer wavelengths could be reached using third order Raman cavities or higher. With currently available fibers, the main limiting factor would be the rising material attenuation near 4 $\mu$m due to the proximity with the S-H bond main absorption peak [17]. In addition, it would also be possible to optimize the coupler reflectivity ($R_{out1}$ and $R_{out2}$) to promote multiwavelength operation of the Raman cavity, as it was done previously with more standard RFLs [18]. The simultaneous emission of 2 or more wavelengths in the mid-IR would be useful for the generation of terahertz waves by the difference frequency in a nonlinear media [19].

## 5. Conclusion

This paper is bringing clear evidence that chalcogenide based RFL can be designed for efficient operation on any wavelength between 3 and 4 $\mu$m. Current bottlenecks of As$_2$S$_3$ Raman fiber lasers include the limited control over the FBGs bandwidth, the use of free-space components to launch the 3 $\mu$m pump power and the presence of OH impurities that increase the attenuation between 2850–3000 nm. In the near future, the FBGs inscription process based on chirped phase mask will be optimized to provide better experimental results. In addition, the replacement of bulk components by an all-fiber solution will be studied to achieve higher power levels.

## References

[1] V. Fortin, M. Bernier, J. Carrier, and R. Vallée, "Fluoride glass Raman fiber laser at 2185 nm," *Opt. Lett.*, vol. 36, no. 21, pp. 4152–4154, Nov. 2011.

[2] V. Fortin, M. Bernier, D. Faucher, J. Carrier, and R. Vallée, "3.7 W fluoride glass Raman fiber laser operating at 2231 nm," *Opt. Exp.*, vol. 20, no. 17, pp. 19 412–19 419, Aug. 2012.

[3] M. Bernier, V. Fortin, N. Caron, M. El-Amraoui, Y. Messaddeq, and R. Vallée, "Mid-infrared chalcogenide glass Raman fiber laser," *Opt. Lett.*, vol. 38, no. 2, pp. 127–129, Jan. 2013.

[4] D. Faucher, M. Bernier, G. Androz, N. Caron, and R. Vallée, "20 W passively cooled single-mode all-fiber laser at 2.8 $\mu$m," *Opt. Lett.*, vol. 36, no. 7, pp. 1104–1106, Apr. 2011.

[5] M. Rini, I. Cristiani, and V. Degiorgio, "Numerical modeling and optimization of cascaded CW Raman fiber lasers," *IEEE J. Quantum Electron.*, vol. 36, no. 10, pp. 1117–1122, Oct. 2000.

[6] J.-C. Bouteiller, "Spectral modeling of Raman fiber lasers," *IEEE Photon. Technol. Lett.*, vol. 15, no. 12, pp. 1698–1700, Dec. 2003.

[7] P. Suret and S. Randoux, "Influence of spectral broadening on steady characteristics of Raman fiber lasers: From experiments to questions about validity of usual models," *Opt. Commun.*, vol. 237, no. 1–3, pp. 201–212, Jul. 2004.

[8] D. V. Churkin, S. V. Smirnov, and E. V. Podivilov, "Statistical properties of partially coherent CW fiber lasers," *Opt. Lett.*, vol. 35, no. 19, pp. 3288–3290, Oct. 2010.

[9] R. Vallée, E. Bélanger, B. Déry, M. Bernier, and D. Faucher, "Highly efficient and high-power Raman fiber laser based on broadband chirped fiber Bragg gratings," *J. Lightwave Technol.*, vol. 24, no. 12, pp. 5039–5043, Dec. 2006.

[10] Y. Feng, L. R. Taylor, and D. B. Calia, "150 W highly-efficient Raman fiber laser," *Opt. Exp.*, vol. 17, no. 26, pp. 23 678–23 683, Dec. 2009.

[11] M. Bernier, M. El-Amraoui, J. F. Couillard, Y. Messaddeq, and R. Vallée, "Writing of Bragg gratings through the polymer jacket of low-loss As$_2$S$_3$ fibers using femtosecond pulses at 800 nm," *Opt. Lett.*, vol. 37, no. 18, pp. 3900–3902, Sep. 2012.

[12] D. Faucher, N. Caron, M. Bernier, and R. Vallée, "QCW all-fiber laser at 2.94 microns," presented at the Fiber Laser Applications, San Diego, CA, USA, 2012, Paper FTh4A.6.

[13] O. P. Kulkarni, C. Xia, D. J. Lee, M. Kumar, A. Kuditcher, M. N. Islam, F. L. Terry, M. J. Freeman, B. G. Aitken, S. C. Currie, J. E. McCarthy, M. L. Powley, and D. A. Nolan, "Third order cascaded Raman wavelength shifting in chalcogenide fibers and determination of Raman gain coefficient," *Opt. Exp.*, vol. 14, no. 17, pp. 7924–7930, Aug. 2006.

[14] C. Xiong, E. Magi, F. Luan, A. Tuniz, S. Dekker, J. S. Sanghera, L. B. Shaw, I. D. Aggarwal, and B. J. Eggleton, "Characterization of picosecond pulse nonlinear propagation in chalcogenide As$_2$S$_3$ fiber," *Appl. Opt.*, vol. 48, no. 29, pp. 5467–5474, Oct. 2009.

[15] M. Asobe, T. Kanamori, K. Naganuma, H. Itoh, and T. Kaino, "Third-order nonlinear spectroscopy in As$_2$S$_3$ chalcogenide glass fibers," *J. Appl. Phys.*, vol. 77, no. 11, pp. 5518–5523, Jun. 1995.

[16] E. M. Dianov and A. M. Prokhorov, "Medium-power CW Raman fiber laser," *IEEE J. Sel. Topics Quantum Electron.*, vol. 6, no. 6, pp. 1022–1028, Nov./Dec. 2000.

[17] A. Andriesh, M. Iovu, O. Shpotiuk, and I. Culeac, "Optical losses and photo-induced absorption in chalcogenide glass fibers," *J. Optoelectron. Adv. Mater.*, vol. 11, no. 12, pp. 2172–2178, Dec. 2009.

[18] M. D. Mermelstein, C. Headley, J.-C. Bouteiller, P. Steinvurzel, C. Horn, K. Feder, and B. J. Eggleton, "Configurable three-wavelength Raman fiber laser for Raman amplification and dynamic gain flattening," *IEEE Photon. Technol. Lett.*, vol. 13, no. 12, pp. 1286–1288, Dec. 2001.

[19] M. Tonouchi, "Cutting-edge terahertz technology," *Nat. Photon.*, vol. 1, no. 2, pp. 97–105, Feb. 2007.